in which case η_R approaches 1 and the fracture energy, E_G, goes to zero as the rupture velocity approaches the shear wave velocity. For about 30 earthquakes of $6.6 < M_W < 8.3$, Venkataraman and Kanamori (2004) obtained radiation efficiency estimates generally between 0.25 and 1.0. One class of earthquakes that appear to have $\eta_R < 0.25$ are *tsunami earthquakes*, which involve slow rupture and generate large tsunamis relative to their moment.

The radiation efficiency should not be confused with the *seismic efficiency*, η, defined as the fraction of the total energy that is radiated into seismic waves:

$$\eta = \frac{E_R}{E} = \frac{E_R}{\overline{\sigma}\overline{D}A} = \frac{\mu E_R}{\overline{\sigma}M_0} = \frac{\mu\tilde{e}}{\overline{\sigma}}. \tag{9.66}$$

The seismic efficiency is more difficult to estimate than the radiation efficiency because it depends upon the poorly constrained absolute stress level on the fault.

In the extreme case where we assume that the earthquake relieves all of the stress on the fault, then $\sigma_2 = 0$ and we say that the stress drop is total. In this case, $E_F = 0$ and we have

$$E_{min} = \tfrac{1}{2}\overline{\Delta\sigma D}A = \frac{\Delta\sigma}{2\mu}M_0. \tag{9.67}$$

This represents the minimum amount of energy release for an earthquake with a given stress drop and moment.

The theories that describe how slip on a fault initiates, propagates, and comes to a halt can be very complicated, even for idealized models with uniform pre-stress and elastic properties. Much of the recent work in this area has involved theory and observations of *rate and state friction* (e.g., Dieterich, 1994) in which the frictional properties are time and slip dependent. Because these models vary in their behavior and it is likely that real earthquakes span a range of different rupture properties, it is important to keep in mind the distinction between parameters that are more-or-less directly estimated (e.g., moment, geodetically-determined static stress drop, and radiated energy) and those that depend upon modeling assumptions (e.g., Brune-type and Orowan stress drops) and thus are not truly independent measurements. For example, it would make little sense to use (9.60) to estimate E_G if both $\Delta\sigma$ and E_R are derived from fitting the observed body-wave spectra to the same theoretical model.

9.7 Earthquake magnitude

For historical reasons the most well-known measure of earthquake size is the earthquake *magnitude*. There are now several different types of magnitude scales, but all are related to the largest amplitude that is recorded on a seismogram. This is one

of the easiest things to measure and is one reason for the continued popularity of magnitude scales. A recent comprehensive review of magnitude scales is contained in Utsu (2002b).

In the 1930s, Charles Richter introduced what is now called the *local magnitude* M_L. This was determined by measuring the largest amplitude A recorded on a standard instrument, the Wood–Anderson seismograph. Richter noticed that plots of log A versus epicentral distance for different earthquakes generally exhibited a similar decay rate (Fig. 9.23). This suggested that a distance-independent measure of earthquake size could be provided by the offset in log A from a reference event at the same range,

$$M_L = \log_{10} A(X) - \log_{10} A_0(X), \tag{9.68}$$

where A_0 is the amplitude of the reference event and X is the epicentral distance. At each seismic station, a value of M_L may be obtained from the measured amplitude A and the value of $\log_{10} A_0$ at the appropriate source–receiver distance (Richter made a table of $\log_{10} A_0$ at different ranges). From the table of values of $A_0(X)$, an approximate empirical formula has been derived (e.g., Bullen and Bolt, 1985):

$$M_L = \log_{10} A + 2.56 \log_{10} X - 1.67, \tag{9.69}$$

where A is the displacement amplitude in microns (10^{-6} m) and X is in kilometers. The formula is valid for $10 < X < 600$ km. For the Wood–Anderson torsion instrument the largest amplitude generally comes from the S-wave arrival. Individual

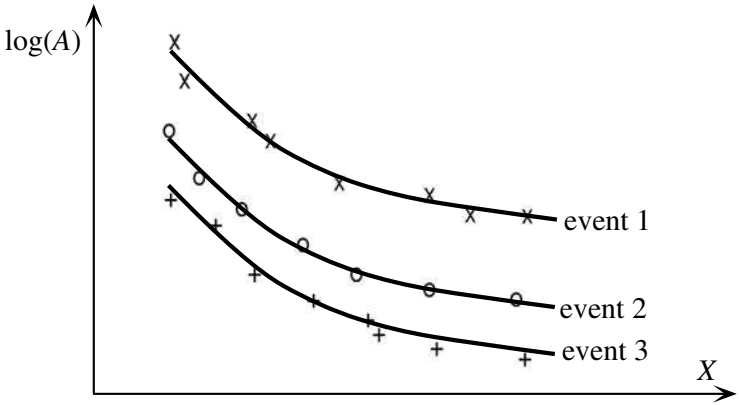

Figure 9.23 Different earthquakes are observed to have a similar falloff in log(amplitude) with distance.

estimates of M_L will exhibit some scatter owing to directivity, radiation pattern, focusing, and other effects. However, a stable estimate can generally be obtained by averaging the results from different stations.

Richter defined a fairly small reference event so that the magnitudes of all but the tiniest earthquakes are positive. Events below about $M_L = 3$ are generally not felt. Significant damage to structures in California begins to occur at about $M_L = 5.5$. The magnitude scale is logarithmic to account for the wide range in observed amplitudes. A $M_L = 6.0$ event implies a recorded amplitude 100 times greater than a $M_L = 4.0$ event.

The Richter magnitude scale provided a practical method of quickly determining the relative size of different events in California. Since the dominant period of the Wood–Anderson intrument (0.8 s) is close to that of many structures, the M_L scale has proven especially useful in engineering seismology. The local magnitude scale is also important because all subsequent magnitude scales have been tied to it. However, the portability of M_L is limited since it is based upon an amplitude versus range relationship that was defined specifically for southern California, and it depends on an intrument that is now rarely used. Caltech and Berkeley kept some Wood–Anderson seismographs operating into the 1990s just to maintain continuity of the magnitude scale. However, these venerable instruments have now been retired since the Wood–Anderson response can be simulated through suitable filtering of modern broadband data. Related to M_L for local earthquakes is the *coda magnitude* (e.g., Suteau and Whitcomb, 1979), which is derived from the amplitude of the scattered waves or coda that follow the direct P and S arrivals, and which has been calibrated to agree with the local magnitude scale. In many cases, coda magnitudes are more stable than M_L because the scattered energy that makes up the coda waves averages out spatial variations and provides a more uniform coverage of the radiation pattern.

A general magnitude scale used for global seismology is the *body-wave magnitude*, which is defined as

$$m_b = \log_{10}(A/T) + Q(h, \Delta), \tag{9.70}$$

where A is the ground displacement in microns, T is the dominant period of the measured waves, Δ is the epicentral distance in degrees, and Q is an empirical function of range and event depth h (e.g., Veith and Clawson, 1972). The Q function includes the details of the average amplitude versus epicentral distance and source depth behavior of the Earth. The measurement is normally made on the first few cycles of the P-wave arrival on short-period vertical-component intruments, for which the dominant wave period is usually about 1 s. As with the local magnitude scale, m_b estimates for the same event will vary between stations, with scatter of up

to about ±0.3. This is due to radiation pattern, directivity, and local station effects. A station correction term is often used to account for stations that consistently give higher or lower m_b values.

Another global seismology scale is the *surface wave magnitude*, which may be defined as

$$M_S = \log_{10}(A/T) + 1.66 \log_{10} \Delta + 3.3 \tag{9.71}$$

for Rayleigh wave measurements on vertical instruments. Since the strongest Rayleigh wave arrivals are generally at a period of 20 s, this expression is often written as

$$M_S = \log_{10} A_{20} + 1.66 \log_{10} \Delta + 2.0. \tag{9.72}$$

Note that this equation is applicable only to shallow events; surface wave amplitudes are greatly reduced for deep events.

The m_b and M_S scales were designed to agree with the M_L scale for local events in California. However, it is not possible to align the scales for all size events. This is because the magnitude scales are obtained at different periods and the frequency content of events changes as a function of event size. Consider the examples in the previous sections, in which the source spectrum falls as f^{-2} above a certain corner frequency. The corner frequency f_c generally moves to lower frequencies for larger events. If we assume stress drop is constant, then the fault dimension and corresponding rupture duration will scale approximately as $M_0^{1/3}$. The corner frequency is inversely proportional to the rupture duration and will scale as $M_0^{-1/3}$. In this case the position of the corner will fall off as f^{-3} (Fig. 9.24).

At frequencies below f_c there is a linear relationship between magnitude ($\log_{10}$ of the measured amplitude) and moment. However, at higher frequencies this linearity breaks down and the magnitude scale does not fully keep up with the increasing size of the events. This phenomenon is called magnitude *saturation*. At a given measurement frequency (e.g., 1 Hz for m_b) this begins to occur when the event size becomes large enough to move the corner frequency below the measurement frequency. Of course, not all earthquake spectra fall off exactly at f^{-2} but any degree of falloff will lead to some saturation of the magnitude scale. Another contributing factor to magnitude saturation can be the fixed window length used to measure the amplitudes, which may not be long enough to capture the true amplitude of larger events (e.g., Houston and Kanamori, 1986). Observed m_b values begin to saturate at about $m_b = 5.5$ and M_S values (measured at longer period) at about $M_S = 8$. For this reason it is rare for m_b to exceed 7 or for M_S to exceed 8.5, even for extremely large events.

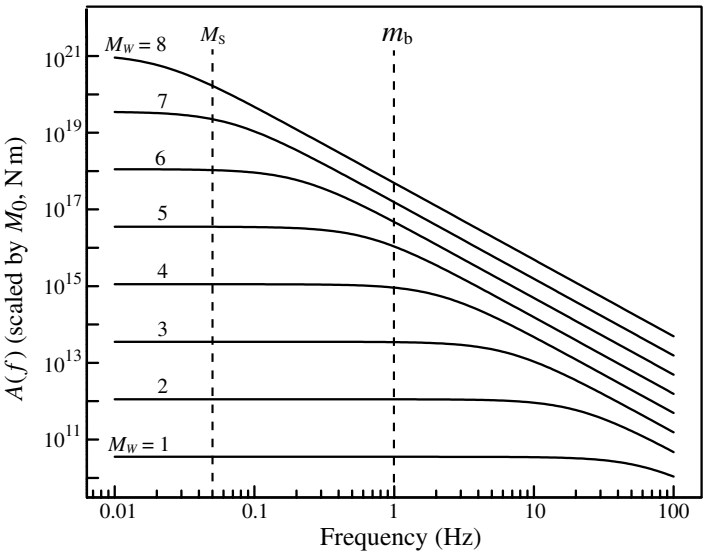

Figure 9.24 For larger events, the corner in the source spectrum moves to lower frequencies, reducing the observed amplitude increase at the fixed frequencies used to estimate M_S and m_b.

The saturation of the m_b and M_L scales for large events helped motivate development of the *moment magnitude* M_W by Kanamori (1977) and Hanks and Kanamori (1979). The moment magnitude is defined as

$$M_W = \tfrac{2}{3}\left[\log_{10} M_0 - 9.1\right], \tag{9.73}$$

where M_0 is the moment measured in N m (for M_0 in dyne-cm, replace the 9.1 with 16.1)[2]. The moment magnitude is derived entirely from the moment, with a scaling such that M_W is in approximate agreement with M_S for many events. The advantage of the M_W scale is that it is clearly related to a physical property of the source and it does not saturate for even the largest earthquakes. It is simply another way to express the moment, which provides units that are easier to quickly comprehend than M_0 numbers like 8.2×10^{19} N m.

However, (9.73) can be misused if it is naively applied to estimate M_0 from an earthquake magnitude. This is because the M_L, m_b, and M_S magnitudes exhibit considerable scatter among events of the same moment and even their average values do not agree with M_W over the full range of event sizes. To see this, consider M_S measurements and the self-similar ω^{-2} source spectra plotted in Figure 9.24.

[2] A minor source of confusion has existed in definitions of M_W, arising from a lack of precision in the final term. The original Hanks and Kanamori paper defined moment magnitude as $2/3 \log M_0 - 10.7$ (dyne-cm). However, many authors, including Aki and Richards (2002), use $\log M_0 = 1.5 M_W + 16.1$, which is slightly different (note that $1.5 \times 10.7 = 16.05$). Additional slight precision loss can occur in translating from dyne-cm to N m because of the 2/3 factor. Here we use the Aki and Richards definition of M_W.

For small earthquakes ($M_W < 6$), the measured amplitude at 20 s will scale linearly with moment and thus $M_S \propto \log_{10} M_0$. For larger earthquakes ($M_W > 8$), the result of the f^{-3} corner frequency falloff and f^{-2} high-frequency spectral falloff is that $M_S \propto \frac{1}{3} \log_{10} M_0$. M_W was defined to agree with M_S mainly for events between M 6 and 8, where a slope of 2/3 is approximately correct. Thus, we should expect M_S to underpredict M_W at both small and large magnitudes. A similar phenomenon should occur for m_b measurements, but shifted to smaller earthquakes because of the higher frequency of the m_b observations.

This is illustrated in Figure 9.25, which plots as gray corridors the distribution of M_S and m_b measurements from the US Geological Survey's Preliminary Determination of Epicenter (PDE) catalog as a function of M_0 values for the same earthquakes from the Global CMT catalog between 1976 and 2005. For reference, the straight line shows M_W values from (9.73), which has a slope of 2/3 on the log plot. M_S agrees approximately with M_W at magnitudes between about 6.5 and 7.5, but underpredicts M_W outside of this interval. The m_b values agree with M_W near magnitude 5, but increasingly underpredict M_W at larger magnitudes. The average m_b and M_S values agree exactly only near magnitude 5.5, where they slightly

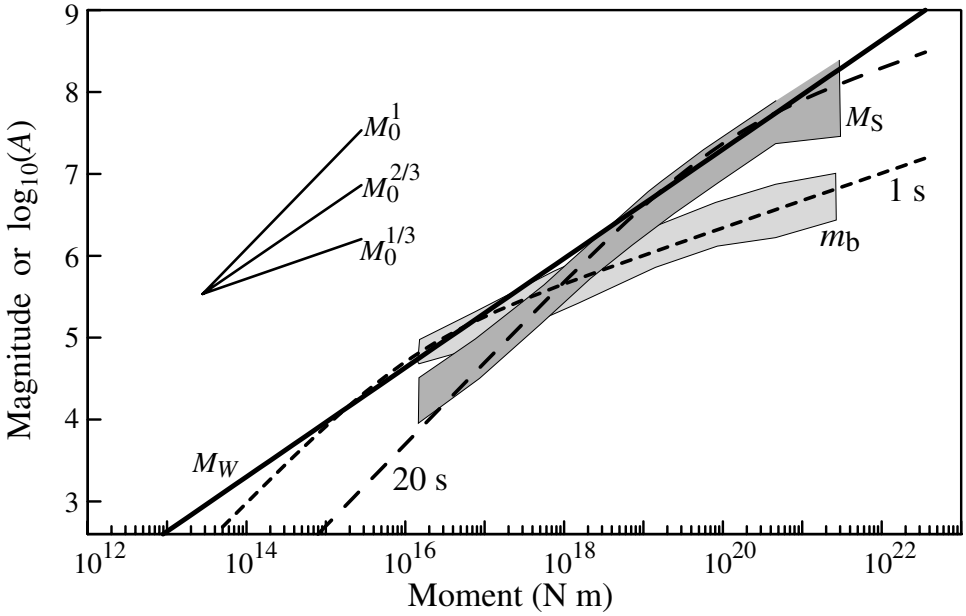

Figure 9.25 Magnitude as a function of moment, M_0, for m_b, M_S, and M_W, compared to predictions of log(amplitude) for an ω^{-2} source model at periods of 1 and 20 s. The gray corridors show m_b and M_S values ($\pm$ one standard deviation) from the USGS PDE catalog versus M_0 from the Global CMT catalog, compared to the definition of M_W (straight solid line). The dashed lines are predicted *P*-wave amplitudes for the Madariaga (1976) source model, assuming a stress drop of 3 MPa.

underpredict the M_W value of 5.8. This behavior can be explained nicely with an ω^{-2} source model, assuming constant stress drop. This model predicts that $\log_{10}(A)$ will vary as M_0 for small events, as $M_0^{2/3}$ for events with corner frequencies near the observation frequency, and as $M_0^{1/3}$ for larger events. Predicted $\log_{10}$ amplitudes at the m_b measurement period of 1 s and the M_S measurement period of 20 s exhibit similar behavior to the data.

Figure 9.25 makes clear how the 2/3 factor in the definition of M_W serves to make M_W values comparable on average to standard magnitudes over a fairly wide range of event sizes, provided m_b is used for earthquakes less than about 5.5 and M_S is used for larger events. However, this correspondence increasingly fails outside of $4 < M_W < 8$. Moment is not routinely estimated for earthquakes below about $M_W = 4$, which are only recorded locally. However, because M_L is computed at a similar frequency to m_b, we should not expect the M_W and M_L scales to agree very well for small earthquakes. Results for the slope of M_L versus $\log_{10}(M_0)$ have varied among different studies, but a systematic analysis of over 60 000 southern California earthquakes of $1 \leq M_L \leq 3$ by Shearer *et al.* (2006) gave a best-fitting slope of 0.96, close to the unit slope predicted from Figure 9.25.

The various seismic magnitude scales are important because they are ingrained in the history and practice of seismology. But if earthquake size is to be quantified with a single number, it is far better to use the moment because it is directly related to a fundamental physical property of the source, which can also be used in geodetic studies of earthquakes and comparisons to long-term geological slip rates. Although it is possible to understand the average behavior of the various magnitude scales with respect to moment, it should be remembered that M_L, m_b, and M_S measurements exhibit large scatter among individual events of the same moment. These differences are presumably not random and may reflect variations in stress drop or other source properties, and appear in some cases to have systematic regional variations (e.g., Ekstrom and Dziewonski, 1988). This is why it is better whenever possible to compute moment directly from the lowest frequency part of the seismic spectra rather than to use magnitude measurements as a proxy for moment.

From (9.73), a one unit increase in M_W corresponds to a $10^{3/2} \simeq 32$ times increase in moment. As we saw in Section 9.6, the average radiated seismic energy is approximately proportional to moment so this means that seismic energy also goes up by a factor of 32. Thus, on average a $M_S = 7$ earthquake releases about 32 times more energy than a $M_S = 6$ event and 1000 times more than a $M_S = 5$ event. This is consistent with the classic empirical Gutenberg-Richter relation between E_R and M_S

$$\log_{10} E_R \text{ (joules)} \simeq 4.8 + 1.5 M_S. \tag{9.74}$$

Table 9.1: Some big earthquakes (M_0 in 10^{20} N m)

Date	Region	m_b	M_S	M_W	M_0
1960 May 22	Chile		8.3	9.5	2000
1964 March 28	Alaska		8.4	9.2	820
2004 Dec 26	Sumatra-Andaman	6.2	8.5	9.1	680
1957 March 9	Aleutian Islands		8.2	9.1	585
1965 Feb 4	Aleutian Islands			8.7	140
2005 March 28	Sumatra	7.2	8.4	8.6	105
1977 Aug 19	Indonesia	7.0	7.9	8.3	36
2003 Sept 25	Hokkaido, Japan	6.9	8.1	8.3	31
1994 Oct 4	Shitokan, Kuriles	7.4	8.1	8.2	30
1994 June 9	Bolivia (deep)	6.9		8.2	26
2004 Dec 23	Macquarie Ridge	6.5	7.7	8.1	16
1989 May 23	Macquarie Ridge	6.4	8.2	8.2	20
1985 Sept 19	Michoacan, Mexico	6.5	8.3	8.0	14
1906 April 18	San Francisco		8.2	7.9	10
2008 May 12	Eastern Sichuan	6.9	8.0	7.9	9
2002 Nov 3	Denali, Alaska	7.0	8.5	7.8	7
2001 Nov 14	Kokoxili, Kunlun	6.1	8.0	7.8	6
1992 June 28	Landers, California	6.2	7.6	7.5	2

However, this agreement is not really a coincidence because this equation was one of the contributing reasons for the 2/3 factor in the definition of M_W (Kanamori, 1977; Hanks and Kanamori, 1979). If we substitute M_W from (9.73) into this equation, we can obtain $E_R/M_0 \simeq 6 \times 10^{-5}$, in rough agreement with the average $\tilde{e}$ values plotted in Figure 9.21, at least over the $6 < M_W < 8$ interval in which $M_W \simeq M_S$. However, it should be emphasized that the radiated energy E_R is best obtained through direct observations; the Gutenberg–Richter relation (9.74) provides a crude estimate, but it can be in error by more than an order of magnitude for individual events.

Table 9.1 lists some of the biggest earthquakes that have been recorded seismically, as well as some smaller strike–slip events for comparison purposes, and Figure 9.26 plots global CMT results between 1976 and 2005, scaled by moment. The listed m_b and M_S values show some of the effects of magnitude saturation. The largest earthquakes of M_W 8.5 and greater occur in subduction zones where the fault area (= length × width) can be very large. Examples include the 1960 Chile earthquake, the 1964 Alaska earthquake, and the 2004 Sumatra-Andaman earthquake.

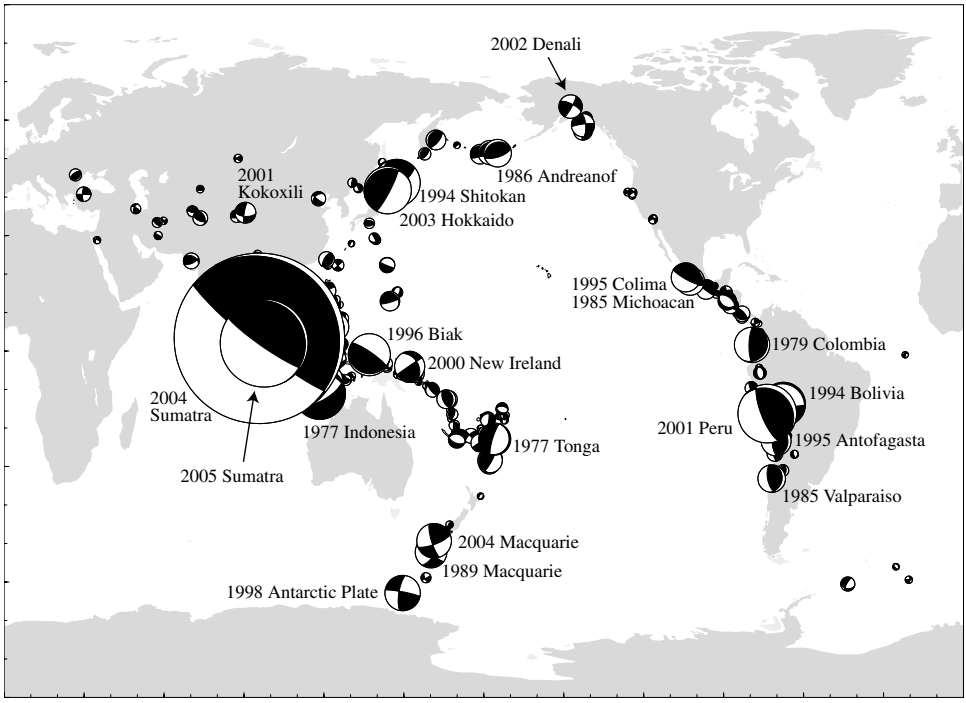

Figure 9.26 The largest earthquakes from 1976 to 2005, with the focal mechanism area proportional to seismic moment, as estimated from the Global CMT catalog.

In contrast, crustal strike–slip earthquakes generally do not exceed about $M_W = 8$ because their fault widths are limited to the upper crust. Recent examples of large strike–slip earthquakes include the 1989 and 2004 Macquarie Ridge earthquakes, the 1998 Antarctic Plate earthquake, the 2001 Kokoxili (China) earthquake, and the 2002 Denali (Alaska) earthquake. Most very large earthquakes are shallow; a notable exception was the 1994 Bolivian earthquake at 630 km depth.

9.7.1 The *b* value

Smaller earthquakes occur much more frequently than large earthquakes. This trend may be quantified in terms of a magnitude–frequency relationship. Gutenberg and Richter noted that this relationship appears to obey a power law[3] and obtained the empirical formula

$$\log_{10} N = a - bM, \tag{9.75}$$

[3] A power-law distribution for earthquake energy had earlier been suggested by K. Wadati.

where N is the number of events with magnitudes greater than or equal to M. In this equation, a describes the total number of earthquakes, while the parameter b is called the *b-value* and measures the relative number of large quakes compared to small quakes. The b-value is generally found to lie between 0.8 and 1.2 for a wide variety of regions and different magnitude scales (for a review, see Utsu, 2002a). As we will discuss in Chapter 10, the b value is often used to estimate the fractal dimension of fault systems (e.g., Aki, 1981; Turcotte, 1997). At $b = 1$ the number of earthquakes increases by a factor of 10 for every unit drop in magnitude. For example, if there is 1 $M = 6$ events per year in a region then we should expect about 10 $M = 5$ events per year, 100 $M = 4$ events, etc.

Figure 9.27 shows $N(M_W)$ computed for the global CMT catalog from 1976 to 2005. Between M_W values 5.5 and 7.5, the distribution is well fit with $b = 1$. At smaller magnitudes the increase in N drops off because earthquakes below about $M_W = 5$ are too small to be well recorded by the global seismic networks. Plots like this are often used to evaluate *catalog completeness* – the lowest magnitude to which a network or catalog includes all of the earthquakes. For $M_W > 7.5$, the numbers also drop below the $b = 1$ line, which may represent a change in the power law or a temporary deficit in the number of very large global earthquakes. Because moment increases by ~30 for every unit increase in M_W, while the number of events only decreases by a factor ~10, the total moment release from all of the seismicity in a region is dominated by the largest events, rather than the accumulated sum of many smaller events. Fortunately for humanity, (9.75) cannot remain valid for

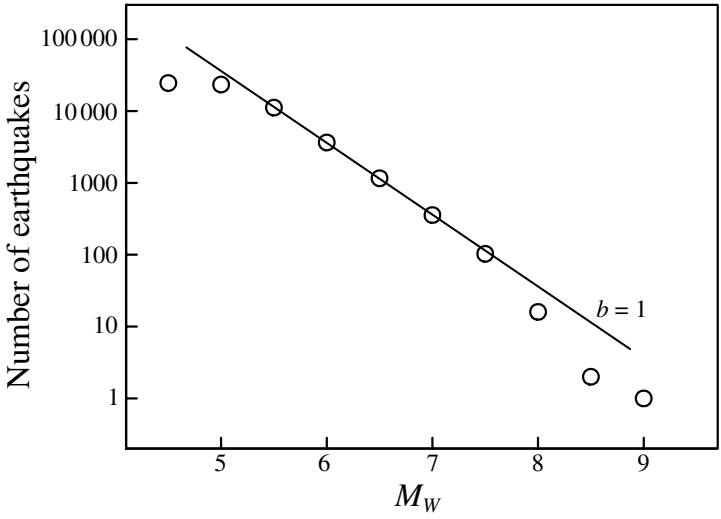

Figure 9.27 $N(M_W)$ for the global CMT catalog from 1976 to 2005, compared to the predictions of a power law decay with b value of 1.

Table 9.2: The modified Mercalli scale, adapted from the abridged version in Bolt (1993).

I	Not felt except by a few under especially favorable circumstances.
II	Felt only by a few persons at rest, especially on upper floors of buildings. Delicately suspended objects may swing.
III	Felt quite noticeably indoors, especially on upper floors of buildings, but many people do not recognize it as an earthquake. Parked cars may rock slightly. Vibration like passing of truck. Duration can be estimated.
IV	During the day felt indoors by many, outdoors by few. At night some awakened. Dishes, windows, doors disturbed, walls make creaking noise. Parked cars rocked noticeably. (0.015–0.02 g)
V	Felt by nearly everyone, many awakened. Some dishes, windows, etc., broken; a few instances of cracked plaster; unstable objects overturned. Disturbance of trees, poles and other tall objects sometimes noticed. (0.03–0.04 g)
VI	Felt by all; many frightened and run outdoors. Some heavy furniture moved, a few instances of fallen plaster or damaged chimneys. Damage slight. (0.06–0.07 g)
VII	Everybody runs outdoors. Damage negligible in buildings of good design and construction; slight-to-moderate damage in well-built ordinary structures; considerable in poorly built or badly designed structures; some chimneys broken. Noticed by people driving cars. (0.10–0.15 g)
VIII	Damage slight in specially designed structures; considerable in ordinary substantial buildings, with partial collapse; great in poorly built structures. Panel walls thrown out of frame structures. Fall of chimneys, factory stacks, columns, monuments, walls. Heavy furniture overturned. Sand and mud ejected in small amounts. Changes in well water. Disturbs people driving cars. (0.25–0.30 g)
IX	Damage considerable in specially designed structures; well-designed frame structures thrown out of plumb; great in substantial buildings, with partial collapse. Buildings shifted off foundations. Ground cracked conspicuously. Underground pipes broken. (0.5–0.55 g)
X	Some well-built wooden structures destroyed; with foundations; ground badly cracked. Rails bent. Landslides considerable from river banks and steep slopes. Shifted sand and mud. Water splashed over banks. (> 0.6 g)
XI	Few, if any, masonry structures remain standing. Bridges destroyed. Broad fissures in ground. Underground pipelines completely out of service. Earth slumps and land slips in soft ground. Rails bent greatly.
XII	Damage total. Waves seen on ground surfaces. Lines of sight and level distorted. Objects thrown upward into the air.

arbitrarily large earthquakes because the finite extent of Earth's faults means there is a maximum possible earthquake size. We need not fear a $M_W = 11$ earthquake every 1000 years.

9.7.2 The intensity scale

Another measure of the earthquake strength is the seismic *intensity*, which describes the local strength of ground shaking as determined by damage to structures and the perceptions of people who experienced the earthquake. The intensity scale most often used today in the United States is the modified Mercalli scale, in which intensity ranges from I to XII (Roman numerals). As shown in Table 9.2, a value of I indicates shaking that is felt only by a few people, V is felt by almost everyone, VIII causes great damage in poorly built structures, and XII indicates total destruction. Although approximate peak accelerations can be assigned to these levels, the great advantage of the Mercalli scale is that it can be used to examine

historic earthquakes that were not recorded by modern instruments. This is often done by interviewing witnesses and studying old newspaper accounts. Once the intensity has been estimated at a number of different sites, a contour map of the intensities can be constructed. The earthquake location is then identified from this map as the spot of maximum intensity, and an approximate magnitude can be estimated from the area surrounded by the different intensity contours. This technique provides the only practical way to obtain probable locations and magnitudes for many older events. The importance of these estimates is illustrated by the seismicity in the eastern United States, where no large earthquake was recorded in the twentieth century. However, several large events occurred in the nineteenth century, including a series of three large earthquakes that struck in 1811–1812 near New Madrid along the Mississippi River in Missouri. By studying and mapping accounts of these events, which were felt across much of the eastern United States, it is possible to constrain their sizes and locations and make estimates of the impact of a future earthquake in the same area. For many years the New Madrid events were thought to be about magnitude 8, but a recent reanalysis of intensity data by Hough *et al*. (2000) indicates that they were more likely M_W 7 to 7.5.

A modern way to quickly estimate earthquake intensities is the "Did You Feel It?" website maintained by the United States Geological Survey (USGS), in which users are asked to answer a short series of questions about how strongly they felt the shaking and to identify their location (http://earthquake.usgs.gov/eqcenter/dyfi.php). These responses are then compiled into an intensity map that can provide surprising detail, as shown in Figure 9.28 for the 2003 M 6.5 San Simeon earthquake in central California. Spatial resolution in the United States is currently limited to zip code boundaries, but in the future it is likely that more precise user locations will make possible more detailed maps.

9.8 Finite slip modeling

Up to this point, we have described seismic sources with a limited number of parameters, such as the moment tensor or focal mechanism, the scalar moment, the duration or corner frequency, the rupture velocity and direction, the stress drop, and the radiated energy. These represent averages over the source region and for small earthquakes this is most of what we can hope to learn because of the limited bandwidth of far-field seismic records. However, for large earthquakes it is often possible to invert for more detailed source properties because it it possible to separately resolve the seismic radiation from different parts of the fault. A common approach is to discretize the fault into a series of rectangular cells, solve for the Green's function that gives the response at each of the available seismic stations,

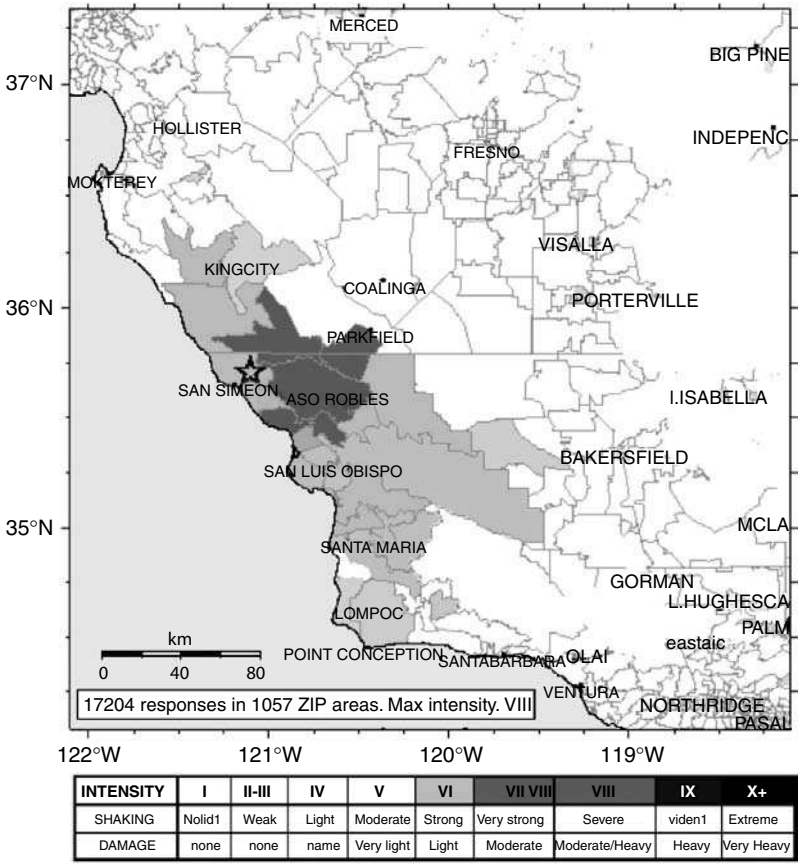

INTENSITY	I	II-III	IV	V	VI	VII VIII	VIII	IX	X+
SHAKING	Nolid1	Weak	Light	Moderate	Strong	Very strong	Severe	viden1	Extreme
DAMAGE	none	none	name	Very light	Light	Moderate	Moderate/Heavy	Heavy	Very Heavy

Figure 9.28 Ground shaking intensities for the 2003 San Simeon earthquake in California, as measured from 17 204 responses to the USGS "Did You Feel It?" website.

and then set up an inverse problem using the superposition principle to solve for the time-dependent slip distribution that best fits all of the data. If geodetic data are also available, these can also be included in the inversion to provide constraints on the total slip. As in the tomographic inversions for 3-D velocity structure discussed in Chapter 5, the inverse problem often is stabilized by applying regularization constraints, such as only permitting slip in one direction and solving for the smoothest or the minimum slip solution.

The resulting *finite slip models* typically show that large earthquakes have irregular slip distributions and that their total moment is dominated by one or two large slip regions where the stress drop is much higher than surrounding parts of the fault. Rupture velocity is also not always constant during earthquakes. As an example, Figure 9.29 shows the Custodio *et al.* (2005) model of the 2004 Parkfield earthquake obtained from an inversion of the strong motion data. From the hypocenter

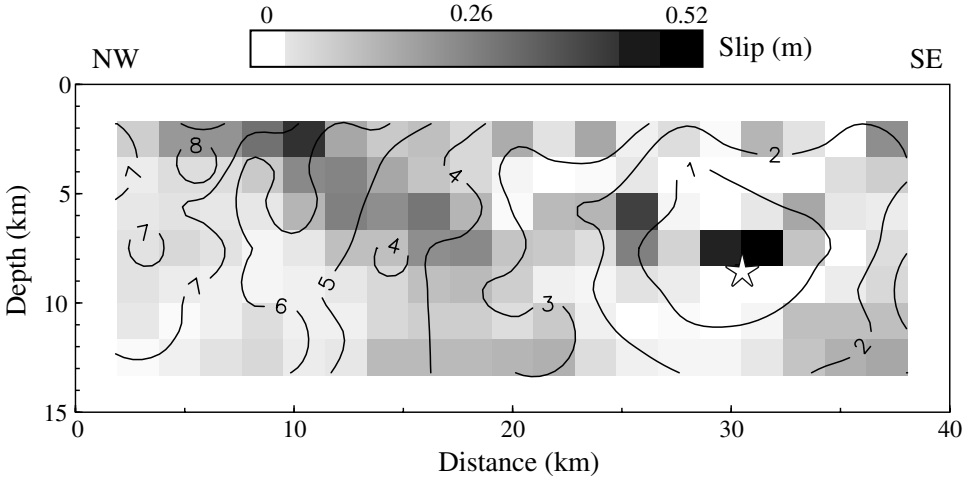

Figure 9.29 The Custodio *et al.* (2005) slip model for the 2004 Parkfield earthquake. The star shows the hypocenter location. The contours show the slip onset times at 1 s intervals.

the rupture propagated northwest along the San Andreas Fault for about 10 s. There were two major areas of slip, one near the hypocenter and the other 10 to 20 km to the northwest at a depth between 2 and 8 km.

Finite slip models provide detailed constraints on rupture dynamics that are valuable for understanding earthquake physics. Results so far point to highly heterogeneous faulting processes with large variations in moment release and stress drop. But there are problems with non-uniqueness in many of the inversions and results from different groups for the same earthquake do not always agree very well. As inversions move to higher frequencies, propagation path effects on strong motion data become increasingly important and link the rupture inversion problem to the 3-D velocity inversion problem. This is an active area of research and eventually improved modeling methods and denser seismic and geodetic networks will help to provide clearer images of fault rupture.

9.9 The heat flow paradox

As discussed in Section 9.6.1, the frictional and fracture energy release during faulting is given by

$$E_{\mathrm{F}} = \sigma_{\mathrm{f}} \overline{D} A \tag{9.76}$$